Design Study of a Side Intrusion Beam for Automotive Safety

Pedro Mota Rebelo
pedro.gomes.mota.rebelo@tecnico.ulisboa.pt

Instituto Superior Técnico, Lisboa, Portugal

November 2016

Abstract

Road safety is one of the major global concerns regarding the protection of human lives. Every year, 1.2 million people die in road related accidents, and 20-50 million suffer from non-fatal injuries. After frontal crash, side impact is the leading cause of road fatalities. Designing safety systems for preventing the accident, or controlling the damages it inflicts on the passengers once it occurs, is a global research subject in which the work developed in thesis is inserted. The side intrusion beam is a protective component installed in the vehicle door, designed to enhance passengers safety in the event of a side collision. This structure's role is to absorb the maximum amount of impact energy through an elasto-plastic deformation process. Thin-walled beams are frequently applied due to their high energy absorption capacity. Metals are commonly selected for the beam design, since they combine a high strength with an also high ductility, both crucial to energy absorption. The present work focuses on studying the impact of the cross-section geometry and material of a thin-walled beam in its bending performance. With a higher bending performance of the side intrusion beam, a better overall performance in a crash event is expected. After significant improvements in bending performance are achieved, the beam solutions are installed in a complete vehicle and tested in different crash configurations. The side intrusion beam is proven to improve the crash performance under specific conditions, for example, during a side pole impact, where the intrusion levels are reduced by the installation of this component.

Keywords: thin-walled beams, energy absorption, bending performance, crash performance, elasto-plastic deformation

1. Introduction

Automotive safety is a major global concern addressed by several organizations worldwide, including the United Nations through its agency World Health Organization. 1.2 million fatalities are registered every year [1] and many more are injured in road accidents. More than one third of the automotive accidents are related with side collisions [2] and about 35% of those accidents are proven fatal [3]. For this reason, designing new and better lateral safety systems is of the outmost relevance. Crashworthiness is the ability of a vehicle to absorb impact energy and protect the vehicle occupants in case of an accident. Cars are designed with multiple protective systems which intend to increase the vehicle crashworthiness. One of those elements is the side intrusion beam (SIB). This element is installed on the vehicle doors and has the main goal of increasing passengers safety during a side crash. Maximizing energy absorption efficiency and attenuating the impact peak force are two crucial factors when designing a side intrusion beam [4]. Energy absorption efficiency means having the lightest beam absorbing the maximum impact energy. Controlling the impact peak force is of very importance as well, since occupant damage may arise from two situations [5]: direct contact between the impactor, or any other car component, and the passenger, or extreme accelerations induced to the human body. The SIB can, in these cases, help preventing the crushing of the occupant compartment and simultaneously induce a slower deceleration of the the impacting vehicle leading to a lower peak force and a softer collision event. In [6] the authors justify that thin-walled beams are the most appropriate solution to the SIB development due to their high reliability and excellent energy absorption capacity. Both [7] and [8] note that thin-walled beams will collapse in bending mode and, for that reason, the bending performance of the SIB becomes a matter of central importance. This thesis focuses on studying the impact of geometry and material selection in a thin-walled beam bending performance. Several configurations are tested in a three-point bending model and their bending performance is evaluated. Finally, the best configurations are selected and in-

stalled in a complete vehicle model to prove the connection between bending and overall crash performances.

2. Background

2.1. Plasticity

During a crash event, the side intrusion beam is subject to large deformations which greatly surpass the elastic limit of the material. In a three-point bending test of a symmetrical beam, the elastic bending equation (1) is only valid for the region closer to the central bending axis where deformations are kept lower for a longer displacement.

$$\sigma = \frac{My}{I} \tag{1}$$

where σ is the normal stress applied to the beam cross-section, M is the pure moment load, I the second moment of area about the neutral axis and y the distance from the bending neutral plane. When the edge of the cross-section (greater y) reaches the yield point, the material starts to deform permanently (plastic deformation). If for the elastic portion of the stress-strain curve, Hooke's linear relationship is generally applied, for the plastic section of the same curve, several models can be used. Let us consider two of these models.

The first model is the elastic, linear-hardening relationship [9]. This model predicts an initial linear elastic behavior according to Hooke's Law and once the yield point is reached, $\sigma = \sigma_0$, where σ_0 is the yield stress of the material, a linear hardening behavior. The linear hardening slope is given as function of the elastic curve,

$$\delta E = \frac{\sigma - \sigma_0}{\varepsilon - \varepsilon_0} \tag{2}$$

where $0 < \delta < 1$ and ε is the material strain and ε_0 is the elastic strain at the yield point. System (3) describes the elastic, linear-hardening model, where the first equation is equivalent to Hooke's Law.

$$\begin{aligned} \sigma &= E\varepsilon \quad (\sigma \leq \sigma_0) \\ \sigma &= (1-\delta)\sigma_0 + \delta E\varepsilon \quad (\sigma \geq \sigma_0) \end{aligned} \tag{3}$$

This model can be expanded to a more complex linear description of the bending behaviour. Considering different slopes $\delta_i, \quad i = 1, 2, 3, ...$, the plastic section of the stress-strain curve can be linearly approximated to the material's actual response.

The second model is a simpler version of the first, and will be used to further develop the study of the plastic bending behavior of a beam. It is the elastic, perfectly plastic relationship [9]. This model predicts a linear elastic behavior according to Hooke's Law until the yield point and then a perfectly plastic behavior, i.e., beyond the yield point the applied stress remains constant whichever the strain applied to the material.

$$\begin{aligned} \sigma &= E\varepsilon \quad (\sigma \leq \sigma_0) \\ \sigma &= \sigma_0 \quad \left(\varepsilon \geq \frac{\sigma_0}{E}\right) \end{aligned} \tag{4}$$

As mentioned before, this is a simpler formulation for the plastic behavior of a material. It is a reasonable approximation for the initial yielding deformation of some metals and is commonly used to perform initial estimations on materials which have a more complex behavior.

In order to obtain a relationship similar to equation (1) but for the plastic bending behavior of the material, the applied force ($\sigma \times Area$) must be integrated throughout the whole cross-section. Considering a rectangular section of height $2c$ and width t, the bending moment is given by

$$M = 2t \int_0^c \sigma y \, \mathrm{d}y \tag{5}$$

Substituting σ and performing a two steps integration, results

$$M = tc^2\sigma_0 \left[1 - \frac{1}{3}\left(\frac{\sigma_0}{E\varepsilon_c}\right)^2\right] \quad (\varepsilon_c \geq \sigma_0/E) \tag{6}$$

where ε_c is the strain at the edge of the cross-section. Figure 1 shows the curve which results from equation (6). In an initial moment, all the cross-section is under elastic deformation. As the strain increases, the elastic region shrinks towards the neutral axis and the perfectly plastic portion grows from the edge of the beam. When the whole cross-section is virtually in a plastic deformation state, the maximum moment is reached and a plastic hinge is formed. The development of plastic hinges is followed by a decrease in load sustaining capacity, thus the maximum load being also called the collapse load. For large values of strain ($\varepsilon_c \gg \sigma_0/E$), equation (6) approaches the fully plastic moment, M_p.

$$M_p = tc^2\sigma_0 \tag{7}$$

Equation (7) shows that the maximum load is highly dependent on both the yield stress and the cross-section area. The development of a plastic hinge on a rectangular beam is illustrated in Figure 2.

2.2. Bending Performance

Four metrics [6] are selected to evaluate the bending performance of the different side intrusion beam configurations:

- *Energy absorption (EA)* – during a bending test or simulation, the applied force is recorded

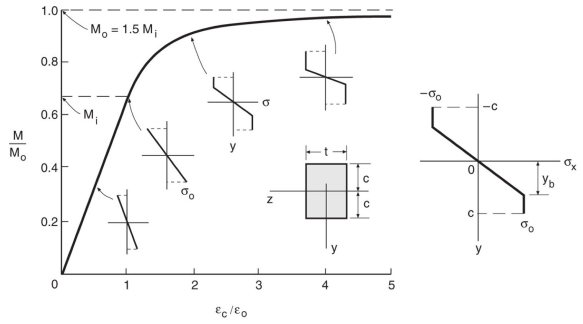

Figure 1: Moment vs. strain behavior for a rectangular beam of an elastic, perfectly plastic material [9]

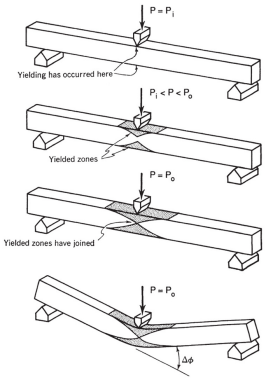

Figure 2: Development of a plastic hinge in three-point bending test [9]

and matched with the imposed displacement. The resulting curve not only shows the magnitude of the exerted force throughout the bending process, but also enables further calculations which lead to the energy absorbed by the beam during its deformation.

$$EA = \int_0^{\delta} F(z)dz, \tag{8}$$

where δ is the imposed displacement and F is the applied force in the z direction.

- *Specific energy absorption (SEA)* – energy absorbed per unit mass

$$SEA = \frac{EA}{M}, \tag{9}$$

where M is the beam's mass.

- *Maximum crash force (F_{max})* – the maximum recorde value of the force/displacement curve

$$F_{max} = \max(F_z) \tag{10}$$

- *Crash force efficiency (CFE)* – ratio between the average applied force and F_{max}

$$CFE = \frac{F_{avg}}{F_{max}}, \tag{11}$$

where F_{avg} is the average crash force which can be expressed as function of the energy absorption parameter and the total displacement,

$$F_{avg} = \frac{EA}{\delta}, \tag{12}$$

This is a comprehensive set which measures force, energy and even an dimensionless figure, the CFE, which transmits the abruptness of the beam bending behavior.

2.3. Regulations

In Europe, lateral impact requirements are regulated by the United Nations Commission for Europe (UNECE) which issued the ECE-R95 regulation[10]. This document presents a detailed lateral crash procedure in order to assess the damage levels inflicted to vehicle passengers. Other institutions, such as EuroNCAP, develop their own procedures and safety criteria, and apply them to the commercially available vehicles, providing the market a more detailed safety profile on each of those vehicles. A side collision impact test and a side pole test will be numerically performed in this thesis, the first based on the ECE-R95 regulation and the latter based on the EuroNCAP procedure [11].

3. Implementation

3.1. Approach

The development of the side intrusion beam will be conducted using a powerful FEA tool, HyperWorks. A complete model of a Geo Metro is used as test basis. However, simulating a crash event with a full vehicle has proven to be time expensive thus, in order to perform an extensive study on several geometries and materials, a simpler and faster model is required. For that reason, a three-point bending model was designed with the intent of assessing the beam's bending performance in a simple low cost simulation. In fact, for side impact, the thin-walled beams will collapse in bending mode [6] which lays a common ground between a complete vehicle side crash simulation and a simple three-point bending test. This model was first validated through experimental testing. Then, different geometries and materials will be tested using the same simulation and performance results will be compared. Concerning material selection, a wide variety of metals will be applied. The combination of high strength with high ductility makes the metal materials a logic option to a scenario where large deformations are expected. Finally, the best configurations are installed and tested in a complete vehicle crash simulation and conclusions are withdrawn regarding the side intrusion beam's overall impact in a side collision.

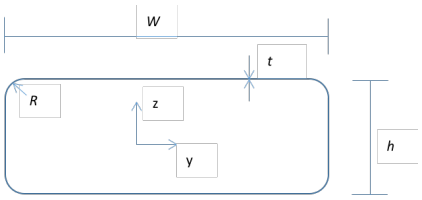

Figure 3: Reference beam

	L_{ref}	R	h	t	W
Dimension (mm)	800	3	25	1.5	50

Table 1: Reference beam data

3.2. Geometry and Material Analysis

This section approaches the development of an improved solution for the design of a side intrusion thin-walled beam. Several geometries and materials will be tested in the three-point bending numerical model validated through experimental testing and their performance results will be compared according to the metrics presented in section 2.2. The validation process is approached in depth in this thesis but will be omitted in this extended abstract. The first step is the definition and analysis of a reference beam, whose cross-section and dimensions are presented in Figure 3 and Table 1, respectively.

In this study, the numerical model is developed with the explicit non-linear finite element code RADIOSS. Figure 4 shows the three-point bending test configuration. The thin-walled beam (length, L) is placed over two identical cylindrical supports (diameter, D). A large span (S) separates both the supports. A cylindrical impactor (diameter, D) pushes the beam downward in its central point at a constant speed (v). The test ends when the target displacement (δ_{max}) is reached. The procedure specifications are displayed in Table 2

$D(mm)$	$S(mm)$	$L(mm)$	$v(mm/s)$	$\delta_{max}(mm)$
30	600	800	500	150

Table 2: Bending test configuration data

Belytschko-Tsay reduced integration shell elements with five integration points through the shell thickness were employed to model the beam. Both the supports and the impactor are considered rigid. Contacts between the impactor and beam, and between the supports and beam were defined to avoid surface penetration. A self-contact is also defined to avoid interpenetration of beam folding during bending collapse. The material applied to the reference beam is a steel grade DP250/450 whose properties are summarized in Table 3. To simulate the material properties, MAT 36 – Elastic Plastic Piecewise Linear Material was used to model elasto-plastic materials according to the second model described in section 2.1. The strain rate effect was neglected as the impact velocity is relatively low [6]. The simulation output is the force/displacement curve of the impactor, from which the metrics described in section 2.2 can be computed.

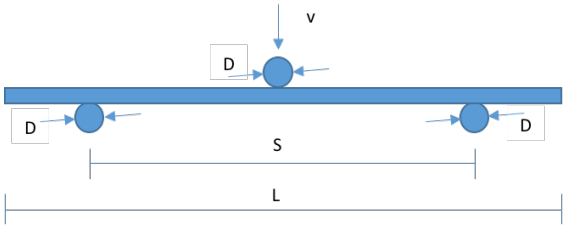

Figure 4: Three-point bending setup

	$\rho(kg/m^3)$	$E(GPa)$	υ	$\sigma_y(MPa)$	$\sigma_{UTS}(MPa)$
DP250/450	8000	210	0.3	250	450

Table 3: DP250/450 properties (Adapted from [12])

Starting from reference beams geometry, a large group of geometrical parameters will be altered in order to understand which solutions have a greater impact on the beam's bending performance. This thesis comprises a comprehensive geometrical study, where several configurations are tested: regular polygons, geometric proportions variation, geometric expansion/reduction, reinforcements introduction, open sections and thickness variation. An additional study is performed to prove that, as long as the strain rate effect can be neglected, the impact speed has almost no effect on the bending performance of a beam. All these analyzes are described in great detail in this thesis. However, in this extended abstract, only the study which showed the best results will be presented, and that is the thickness variation analysis.

This analysis studies the effect of thickness variation in the bending performance of the reference beam. Four different thickness values (including the reference t) are evenly applied through the cross-section. In a thin-walled beam the thickness of both the webs and the flanges are expected to have a great impact in the beam's bending performance. Thickness variation configurations are illustrated in Figure 5 and the geometrical dimensions are specified in Table 4. The numerical model used is identical to the one applied on the reference beam.

Finally, a material analysis is performed. Several metal materials are applied to the reference beam under the same three-point bending test whose specifications were previously described. Three metal types were selected: steel, aluminum

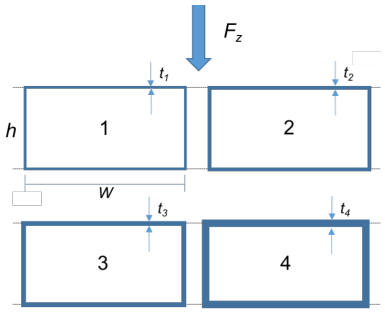

Figure 5: Thickness variation loading scenarios

	h	W	t_1	t_2	t_3	t_4
Dimension (mm)	25	50	0.5	1.5	3	5

Table 4: Thickness variation geometrical parameters values

and titanium. A full list of the used materials (including the reference material DP250/450) and their respective properties is presented in Table 5, where ε_R represents the elongation at break, or fracture strain. The properties ρ, E and υ for all the steel grades referenced from [12] are approximated, since no exact values were available. These materials' stress-strain curves are omitted in this extended abstract, but are presented in the full version of the thesis.

3.3. Crash Tests

After testing and evaluating the bending patterns of different configurations, the two solutions with a higher performance are selected to perform the simulation of two crash procedures: side collision impact test and side pole test. This last analysis is intended to study the relationship between bending and overall crash performances. An improved solution, i.e., with a higher bending performance, is expected to provide greater safety levels to vehicle passengers. The lack of a dummy model limits the damage information that may be retrieved from this numerical model. Thus, in order to analyze the behavior of different beams, a comparative study will be conducted in this section. First, the vehicle is crashed with the reference beam. Then, both beam configurations are tested and, finally, a no-beam configuration is also tested. These several analyzes will show, first, how an improvement in bending performance relates with the full vehicle crash behavior, and second, what role the reference beam plays, when compared to a no-beam configuration.

The force/displacement curve will not be used to assess energy absorption since there is no exact way of recording which amount of force is directly applied on the beam. Instead, a displacement analysis on the door's inner panel will be performed to understand which solutions predict a smaller intrusion from the external object into the passengers compartment. Despite being far from the required damage assessments, this method provides a simple way of testing, in a crash event, how a more rigid beam behaves and what impact that behavior has on the intrusion of an external object. This is a ver limited approach, but once again, the purpose of this section is to confirm wether or not an improved beam configuration displays a better performance in a crash scenario.

A Geo Metro detailed model, MetroD, is used to perform the crash tests. This model has been developed by the NCAC [16] and is composed by 193200 finite elements, including 1D, 2D and 3D configurations. It is validated for crash analyzes ran on the solver LS-DYNA. HyperCrash is able to convert the LS-DYNA file into an equivalent RADIOSS extension, and the model is assumed to remain valid. The MetroD model is illustrated in Figure 6 and its main dimensions are provided in Table 6, where M_m is the vehicle's mass. The side intrusion beam is installed inside the MetroD's door as illustrated in Figure 7.

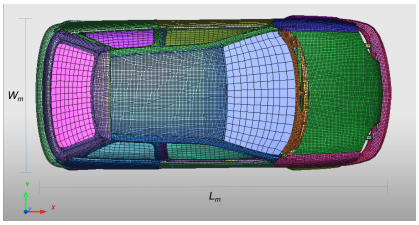

(a) Top view

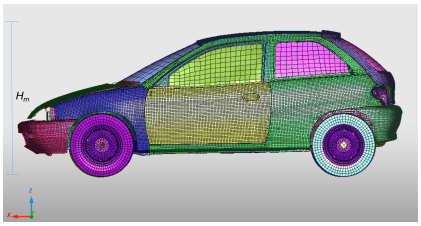

(b) Side view

Figure 6: Geo Metro finite element model

The numerical model is once again developed with the explicit non-linear finite element code RADIOSS. The impacting objects are placed as close as possible to the vehicle in order to save computational time and the simulation is recorded during $0.06s$. This period is long enough to observe a considerable displacement and limits the computational cost to acceptable values. As previously mentioned, the intrusion level will be measured through the displacement curves (in the impact direction, y) of the door's inner panel. In order to evaluate such

		$\rho(kg/m^3)$	$E(GPa)$	υ	$\sigma_y(MPa)$	$\sigma_{UTS}(MPa)$	$\varepsilon_R(\%)$
Steel	DP250/450 [12]	8000	210.0	0.30	250	450	32
	HSLA350/450 [12]	8000	210.0	0.30	350	450	27
	FB450/600 [12]	8000	210.0	0.30	450	600	17.5
	CP650/850 [12]	8000	210.0	0.30	650	850	13.5
	TWIP750/1000 [12]	8000	210.0	0.30	750	1000	37
	TWIP950/1200 [12]	8000	210.0	0.30	950	1200	20
Aluminum	Al2014-T6 [13][14]	2800	72.4	0.33	414	483	12
	Al5086-H32 [13][14]	2660	71.0	0.33	207	326	12.4
	Al6061-T65 [13][14]	2700	68.9	0.33	276	303	15
	Al7075-T62 [13][14]	2810	71.7	0.30	503	621	11
Titanium	Ti-6Al-4V [14][15]	4430	113.8	0.34	880	1009	11

Table 5: Materials list and respective properties (Adapted from [12][13][14][15])

	$L_m(mm)$	$W_m(mm)$	$H_m(mm)$	$M_m(kg)$
Geo Metro	3750	1550	1430	592

Table 6: Geo Metro main dimensions

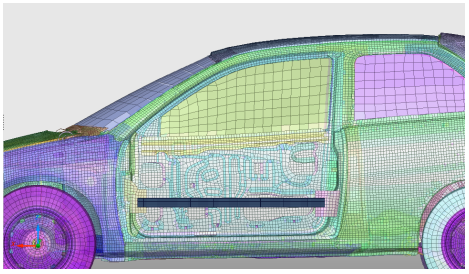

Figure 7: Side intrusion beam installed inside the door

displacement, a wide set of nodes divided into five horizontal levels is selected throughout the door. These levels cover the most critical door regions providing an overall accurate description of the inner panel's deformation pattern. The specific location of such nodes is illustrated in Figure 8 and detailed in Table 7. The two crash procedures differ mainly on two key parameters: impactor configuration and impact velocity.

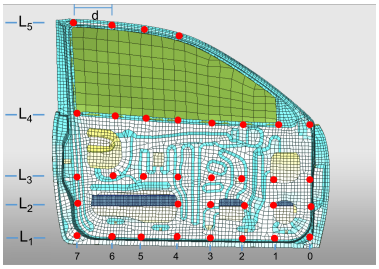

Figure 8: Selected nodes from the inner panel

	Location	Ground Distance(mm)
L_1	Sill top	360
L_2	Occupant H-point	500
L_3	Mid-door	640
L_4	Window sill	900
L_5	Window top	1300
d	–	140

Table 7: Parameters of Figure 8

3.3.1 Side Impact Collision Test

This first procedure is based on the ECE-R95 regulation [10] and studies the impact of a moving deformable barrier against the tested vehicle. As a simplification, this barrier is considered rigid and only the impactor geometry is modelled, where all the mass ($M_{mdb} = 950kg$) is concentrated. It is accelerated with an initial velocity $v_i = 13888.9mm/s$ or $v_i = 50km/h$ perpendicular to the vehicle longitudinal axis. The barrier is centered with the passenger R-point whose position is estimated being $135mm$ away from the B pillar to the front of the vehicle and its dimensions are specified in the regulation. The complete setup is illustrated in Figure 9.

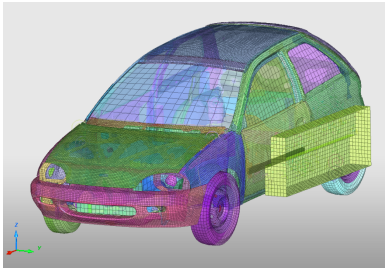

Figure 9: Side impact collision global setup

3.3.2 Side Pole Test

This procedure is based on directives from EuroNCAP [11] and studies the impact of the tested

vehicle against pole-like structures, such as sign-posts or trees. In this procedure, the vehicle is accelerated against a rigid and static pole with a $v_i = 8888.9mm/s$ or $v_i = 32km/h$ directed with an angle of 75^o in relation to the vehicle longitudinal axis. The pole dimensions and positioning are detailed in [11], but essentially, it has to cover all the vehicle's height and the first point of impact must be directed towards the passenger's center of gravity. The complete setup is illustrated in Figure 10.

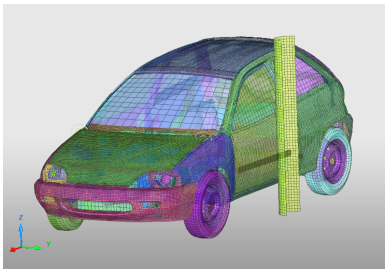

Figure 10: Side pole global setup

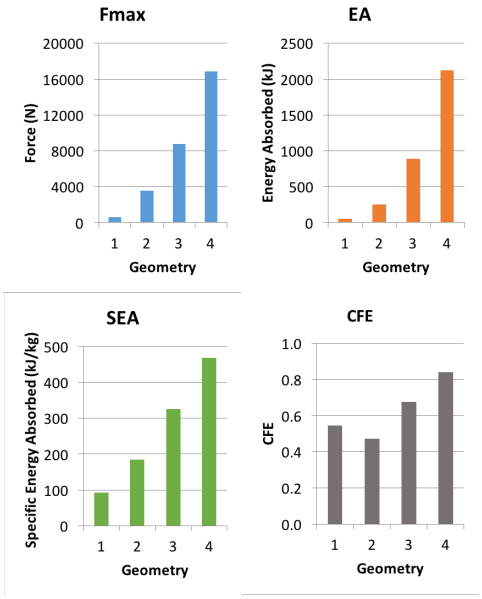

Figure 11: Thickness variation bending performance metrics

4. Results

4.1. Geometry and Materials

Figure 12 shows the force/displacement curves for the thickness variation analysis. Note that beam 2 is equivalent to the reference beam. Figure 11 shows the bending performance results for the four different configurations.

As expected, thickness variation plays a determinant role regarding beam bending performance. Thickness increase leads to a greater F_{max}, EA, SEA and CFE (with the exception of an initial drop from beam 1 to beam 2). A greater F_{max} is a direct consequence of the the greater cross-section area, as showed by equation (7). The higher energy absorption, however, is a consequence of a greater F_{avg}. The bending pattern of the beam varies significantly with the thickness increase. For lower thickness values (reference beam included) the curve displays an initial peak force value, followed by an abrupt drop in load sustaining capacity. As thickness is increased, this pattern is altered. No only the peak force is only reached after a greater displacement, but more importantly, it is not followed by the sudden drop recorded for thinner walls. The combination of these two factors lead to a greater crash force efficiency, CFE, and to a greater specific energy absorption, SEA, i.e., to a greater energy absorption per unit mass. Overall, a greater SEA value combined with a greater mass result in a much greater energy absorption capacity, EA, thus a better bending performance. Comparing the $5mm$ thick configuration with the reference beam, an increase of over 740% in the EA metric is recorded. This was the best bending performance improvement registered in this thesis. Nevertheless, it is followed by an 233% increase in mass, thus the importance of knowing the project requirements when selecting an appropriate solution. Understanding the change in the bending pattern of the beam is very important. The maximum force, or collapse load, is marked by the development of plastic hinges, described in section 2.1. Once these hinges are formed, the cross-section will more easily fold over these lines and the load sustaining capacity decreases. This behavior is transversal to every geometry and material under a bending test. Delaying the development of these plastic hinges is the key to obtain a better bending performance. When the wall thickness is increased, not only the fully plastic moment is higher, but also the development and propagation of these hinges is slowed down. The structure becomes more rigid and more energy is absorbed during the deformation process.

Figure 14 shows the force/displacement curves for the materials analysis. Note that beam 1 is equivalent to the reference beam. Figure 13 shows the bending performance results for the four different configurations.

Analyzing Figure 14, the three metal groups, steel, aluminum and titanium, are easily identifiable by the initial slope of the respective force/displacement curves. Since the initial deformation of the beam occurs in an elastic state, where by Hooke's Law, the stress is proportional to the strain, a larger E value for the steel grades justifies the higher slope registered in the force/displacement curves. Despite having different materials with several different properties, the

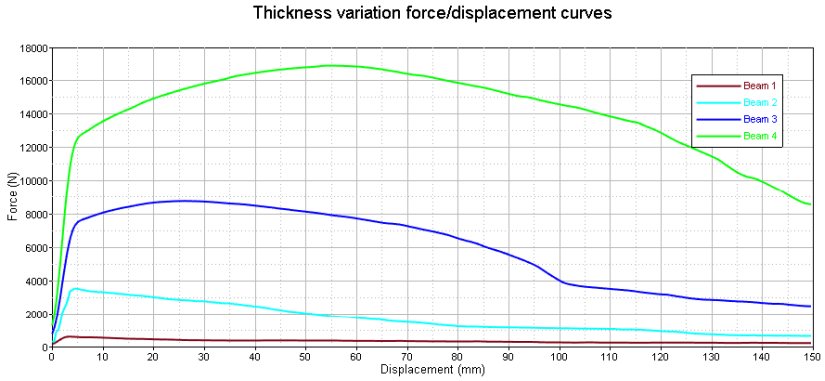

Figure 12: Thickness variation force/displacement curves

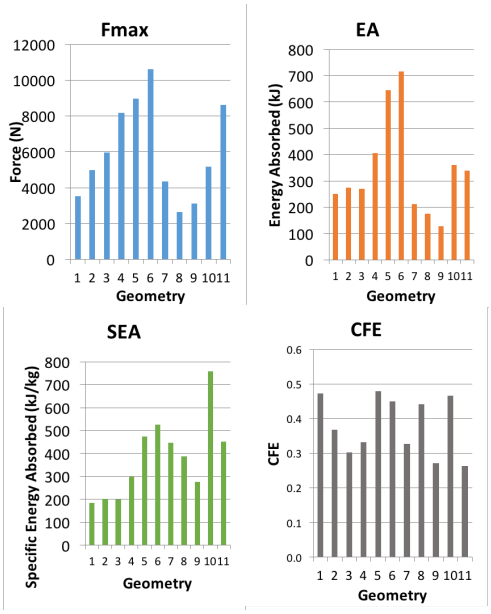

Figure 13: Materials bending performance metrics

force/displacement curve always presents an initial peak configuration followed by a sudden drop in load sustaining capability. This leads to the conclusion that the bending pattern does not depend on the material as much as it depends on the cross-section geometry. The metrics, however, vary significantly depending on the material selection. Comparing F_{max} results with the yield stress of each material, it is clear that they are both highly related. The rectangular geometry exhibits an initial force peak, related to the starting deformation process. During this early stage of the simulation, a great portion of the solicited region of the beam is still in an elastic state. Requiring a higher stress to transition to a plastic state, the materials with higher σ_y demand a greater effort from the impactor to impose the same displacement. The TWIP grades have the highest yield points and ultimate tensile strength, which lead to a higher peak force and energy absorption. Nevertheless, the steel grades approximate density is much higher than the density of the aluminum. Combining a tensile yield strength over $500MPa$ with a low density which represents only 35% of a traditional steel, the Al7075 grade has the highest SEA value by a margin 44% when compared to the next best performer, the TWIP950/1200. The titanium grade is not an appropriate choice due to its elongation at break, 11%, which induces a rapid decrease in load sustaining capacity, thus diminishing the energy absorption and the crash force efficiency. TWIP950/1200 has the best bending performance of all the tested solutions, with an EA value 186% higher than the reference beam's.

Both the $5mm$ thick beam, herein called $Beam5$, and the reference geometry with a TWIP950/1200 grade applied, herein called $Beam950$, were the selected configurations to be tested in the two crash scenarios.

4.2. Crash Test

A fully detailed description of the crash test results is presented in the thesis. In this extended abstract, the main results and conclusions are summarized. For that reason, and despite having been recorded the displacement for all the nodes illustrated in Figure 8, only the results relative to level two (L2), registered in the instant $t = 0.04s$ are discussed. Level two was selected due to its location close to the side intrusion beam, where the greatest intrusion variations are measured, and this time frame is particularly relevant since it provides an accurate description of the overall crash performance.

4.2.1 Side Impact Collision

Figure 15 shows the displacement in the impact direction y of the inner panel's level two of the MetroD model's door at the time frame $t = 0.04s$, for the side impact collision test. $Beam5$, the more rigid beam, displays the greatest intrusion, as the

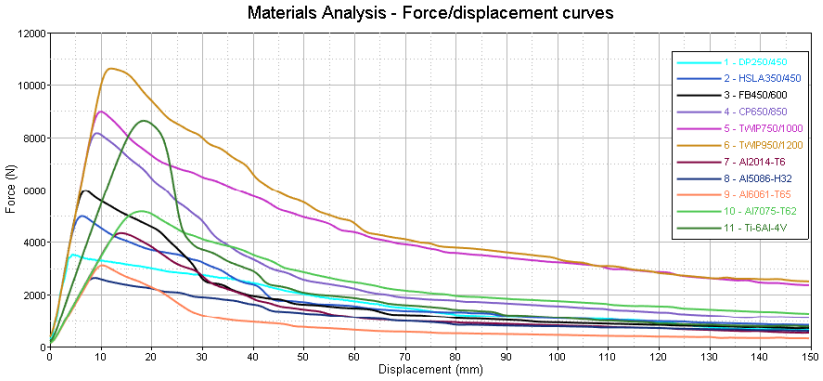

Figure 14: Materials force/displacement curves

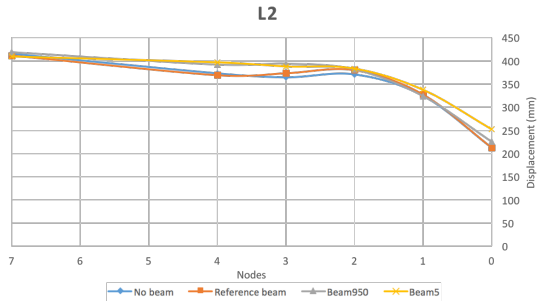

Figure 15: Panel deformation at level two, $t = 0.04s$, in a side collision impact test

no beam configuration, displays the lowest. These results are transversal through all levels during the entire simulation and show that a better bending performance leads to an overall worse crash performance. The panel which has $Beam5$ installed actually deforms less than the the remaining ones, which is visible by a lesser difference between the initial (node 0) and final (node 7) displacement values. However, the increased rigidity is responsible for this greater intrusion due to two main factors: first, as the beam requires greater loads to bend, those same loads are transferred to the beam fixation points, which collapse, leading to a greater intrusion of the whole door assembly; second, the increased rigidity leads to load concentration phenomenon transferring part of the impact energy, otherwise used in the deformation of the rear part of the vehicle, to the door region. This second factor is visible by the smaller displacement registered in the region which precedes the vehicle door, best illustrated in Figure 16 at time frame $t = 0.02s$.

4.2.2 Side Pole Test

Figure 17 shows the displacement in the impact direction y of the inner panel's level two of the MetroD model's door at the time frame $t = 0.04s$, for the side pole test. $Beam5$ displays the smaller deformation, followed by $Beam950$, the reference beam and, finally, the no beam scenario. Here, the improvements in bending performance translate in a better overall crash performance. A more rigid solution prevents, not only the deformation of the inner panel, but also the overall intrusion of the external object. Figure 17 represents only a particular level, but the same bending pattern is observed throughout the whole panel. In this procedure, the concentrated load applied by the impactor is distributed by the beam, which has the opposite role when compared to the side collision impact test, when this component was responsible for a load concentration in the critical region. Overall, in a side pole it is proved that the side beam prevents the intrusion of the external object, and that an improvement in the beam bending performance results in a better crash response.

5. Conclusions

Relatively to bending performance improvement, it is showed that thickness variation of the thin-walled beam plays a major role in enhancing EA capacity, delaying the development of plastic hinges in the more solicited areas. Material selection also plays a crucial role, specially its yield stress, σ_y, which influences directly the maximum bending load the beam can sustain. The bending pattern, however, is barely influenced by material selection, being a characteristic of the geometry itself.

The use of a side intrusion beam in a crash event is proven to be beneficial in a side pole test, where the concentrated load is distributed by the beam, and prejudicial in a side collision impact test, where the beam concentrates an, otherwise, distributed load in the critical door region leading to a more severe intrusion.

Acknowledgements

I would like to thank CEIIA for all the support, both technical and scientific, which made possible the development of this thesis.

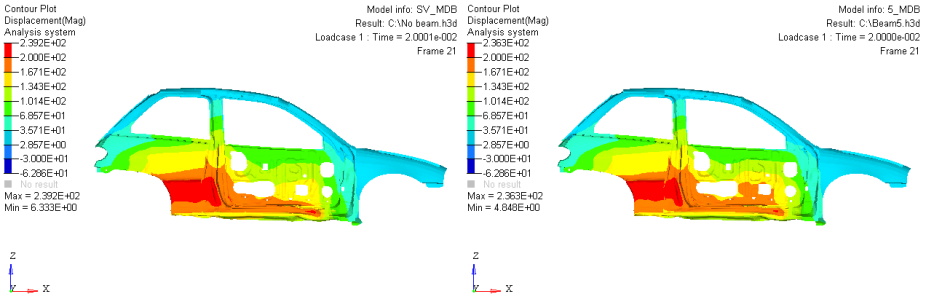

Figure 16: Front and rear extended analysis of the impact displacement at $t = 0.02s$

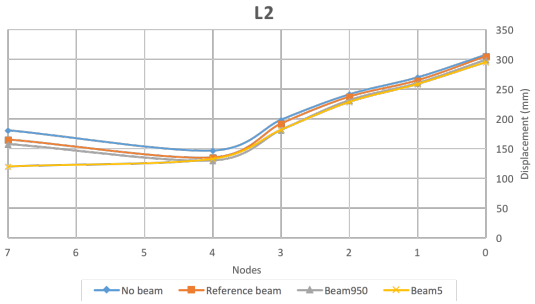

Figure 17: Panel deformation at level two, $t = 0.04s$, in a side pole test

References

[1] A. Shalom Hakkert and Victoria Gitelman. Thinking about the history of road safety research: Past achievements and future challenges. *Transportation Research Part F*, 25:137–149, October 2014.

[2] Ali Ghadianlou and Shahrir Bin Abdullah. Crashworthiness design of vehicle side door beams under low-speed pole side impacts. *Thin-Wallled Structures*, 67:25–33, March 2013.

[3] E. Černiauskas, A. Keršys, V. Lukoševičius, and J. Sapragonas. Investigation of anti-intrusion beams in vehicle side doors. *Mechanika*, 6(86), January 2010.

[4] Xiong Zhang, Hui Zhang, and Zong Wang. Bending collapse of square tubes with variable thickness. *International Journal of Mechanical Sciences*, 106:107–116, 2015.

[5] Fred Preston and Ray Shortridge. An evaluation of the effectiveness of side – door beams based on accident exposure. Special Report 1973 UM-HSRI-SA-73-8, Highway Safety Research Institute, September 1973.

[6] Tao Tang, Weigang Zhang, Hanfeng Yin, and Han Wang. Crushing analysis of thin-walled beams with various section geometries under lateral impact. *Thin-Walled Structures*, 102:43–57, January 2016.

[7] Weigang Chen. Experimental and numerical study on bending collapse of aluminum foam-filled hat profiles. *Int. J. Solids Struct*, 38(44):7919–7944, 2001.

[8] Zonghua Zhang, Shutian Liu, and Zhiliang Tang. Design optimization of cross-sectional configuration of rib-reinforced thin-walled beam. *Thin-walled Struct*, 47(8):868–878, 2009.

[9] Norman E. Dowling. *Mechanical Behavior of Materials – Engineering Methods for Deformation, Fracture and Fatigue*. Prentice-Hall International Editions, 1993.

[10] United Nations Economic Commission for Europe. *Addendum 94: Regulation No.95*, February 2014.

[11] European New Car Assessment Programme. *Oblique Pole Side Impact Testing Protocol*, November 2015.

[12] World AutoSteel. *Advanced High-Strength Steels Applications Guidelines Version 5.0*, May 2014.

[13] ASM International. *Metals Handbook – Properties and Selection: Nonferrous Alloys and Special-Purpose Materials*, volume 2. 10 edition, 1990.

[14] United States of America Department of Defense. *Metallic Materials and Elements for Aerospace Vehicle Structures*. 2003.

[15] R. Boyer, G. Welsch, and E. W. Collings. *Materials Properties Handbook: Titanium Alloys*. 1994.

[16] National crash analysis center. `https://web.archive.org/web/20150415013506/http://www.ncac.gwu.edu/vml/models.html`. [Accessed November 2016].